# Optical conductivity in ferropnictides with and without gap nodes

J. P. Carbotte[1,2] and E. Schachinger[3,*]
[1]*Department of Physics and Astronomy, McMaster University, Hamilton, Ontario, Canada N1G 2W1*
[2]*The Canadian Institute for Advanced Research, Toronto, Ontario, Canada M5G 1Z8*
[3]*Institute of Theoretical and Computational Physics, Graz University of Technology, A-8010 Graz, Austria*
(Received 3 December 2009; revised manuscript received 11 February 2010; published 10 March 2010)

The real part of the optical conductivity of a superconductor with an extended *s*-wave gap as well as the corresponding reflectance and optical scattering rate are calculated within BCS theory. We consider the case when gap nodes exist in certain directions on the Fermi surface and when there is instead a finite spectral gap everywhere. When nodes exist they can be lifted by increasing disorder. Static residual impurities wash out anisotropy and produce a finite gap in all momentum directions before eventually becoming isotropic. This provides a mechanism for the emergence of an additional gap energy scale, the magnitude of which can be tuned through the control of the elastic scattering. Application to the ferropnictides is discussed within a two-band model with the aim of identifying signatures of nodes and of node lifting when several bands are involved.

DOI: 10.1103/PhysRevB.81.104510 PACS number(s): 74.25.N−, 74.20.Rp, 74.25.F−, 74.70.−b

## I. INTRODUCTION

With the discovery of new superconducting materials comes the possibility that phenomena, not observed in conventional systems, could become realized. The layered ferropnictides found only recently[1] display complex band structures[2] with several electronlike or holelike pockets crossing the Fermi surface and represent a further example of multiband superconductivity. Unlike $MgB_2$ which is a two-band electron-phonon system,[3–5] these materials are not electron-phonon driven[6] and may involve a spin-fluctuation mechanism as is likely to be the case in the high-$T_c$ cuprates, although as yet there is no consensus on this issue.

A minimum band-structure model for the ferropnictides involves two bands: an electron ($\beta$) band at the M point and a hole ($\alpha$) band centered at the $\Gamma$ point of the Brillouin zone with *s*-wave gaps on each pocket and possibly a sign change between them,[7,8] the so-called $s^{\pm}$ symmetry state. Other states with *d*-wave symmetry have also been considered and found in some models to be nearly degenerate[9–12] with the *s*-wave case. Also in the $s^{\pm}$ model, the gap on the electron ($\beta$) pocket could be extended *s* wave rather than constant (isotropic *s* wave) and have nodes on its Fermi surface.[13] To put this possibility in perspective, we recall that in conventional superconductors, the electron-phonon interaction is highly anisotropic,[14–17] although there are no nodes. Disorder washes out this anisotropy and for impurity-scattering rates large as compared with the gap amplitude most properties can be described with isotropic *s*-wave BCS theory. Further, once the gap becomes isotropic, impurity scattering drops out of the gap equation. The case of high-$T_c$ cuprates with *d*-wave gap symmetry is very different. While the gap can involve many higher harmonics[18–24] and not just the lowest-order *d* wave, impurity scattering does not change its symmetry and a node will remain even as the gap amplitude is driven to zero and superconductivity is lost. Ordinary impurities work very much the same way in a *d*-wave superconductor as do magnetic impurities in the *s*-wave case.[25] The situation is again different in the ferropnictides with extended *s*-wave symmetry. We can model the total gap on the electron pocket, for example, as the sum of an isotropic constant part plus a *d*-wave component which provides the variation with momentum direction on the Fermi surface. A node results when the *d*-wave component can overcompensate for the *s*-wave component in some specific directions. As impurities are added, the *s*- to *d*-wave admixture changes and the anisotropy decreases. Before isotropy is reached, however, there will be a point at which no nodes remain and we see the emergence of an additional energy scale associated with a finite spectral gap everywhere on the Fermi surface. This lifting of gap nodes by disorder in an extended *s*-wave superconductor was recently considered by Mishra *et al.*[26] with particular emphasis on its consequences for the temperature dependence of the London penetration depth. With gap nodes, one gets a low-temperature power law while exponentially activated behavior signals the existence of a gap in the charge-carrier excitation spectrum out of the superconducting zero-temperature ground state. At the moment, both behaviors are observed in the ferropnictides, sometimes even in nominally similar samples, a situation which, in part, motivated the work of Mishra *et al.*[26] These authors also note discrepancies between results obtained with different probes on the same material. A detailed analysis[27] of the microwave data by Hashimoto *et al.*[28] found that it could be most naturally understood with an extended *s*-wave gap with nodes on the electron pocket but that the temperature dependence of the penetration depth by the same authors was more consistent with no nodes. A separate London penetration depth study by Martin *et al.*[29] on a closely related sample, however, did indicate nodes. The question of nodes or lack there of in the extended *s*-wave gap in the ferropnictides is, thus, central to an understanding of their superconducting properties.

Optics provides detailed information on charge-carrier dynamics and can, in principle, be used to probe superconducting gap anisotropy. Because it is a spectroscopy, a spectral gap (at energy $\omega_g$) in the charge-carrier excitation spectrum should manifest itself as a rise in absorption at twice this energy ($2\omega_g$) as is well known from the work of Mattis and

 

Bardeen.[30] This information is complementary to that on the temperature dependence of the penetration depth, microwave response, and nuclear-magnetic-resonance (NMR) relaxation rate recently discussed by Dolgov *et al.*[31]

In this paper, we report results of calculations for the optical conductivity of an extended *s*-wave gap with nodes within BCS theory and consider the effect of increased impurity scattering. In Sec. II, we present the necessary formalism and give formulas from which the optical conductivity can be calculated numerically. We present numerical results on the quasiparticle density of states (DOS) and show its evolution with increased disorder. In Sec. III, we give results for the real part of the optical conductivity $\sigma(T,\omega)$ and for the reflectance itself. We also introduce the optical self-energy which is derived from an extended Drude form for $\sigma(T,\omega)$ and give numerical results for the optical scattering rate. Section IV is specific to the ferropnictides and discusses how nodes and the lifting of these nodes would present itself in a two-band system. A short summary and conclusions are found in Sec. V.

## II. OPTICAL CONDUCTIVITY

For simplicity, we begin with an anisotropic gap of the form[32] $\Delta_{sd}^0=\Delta_s^0+\Delta_d^0\sqrt{2}\cos(2\phi)$, where $\phi$ is a polar angle on the two-dimensional circular Fermi surface. The constant part is taken as $\Delta_s^0=\alpha\Delta_0$ and the angular-dependent part as $\Delta_d^0=\sqrt{1-\alpha^2}\Delta_0$ so that $\Delta_0=\sqrt{\langle(\Delta_{sd}^0)^2\rangle_\phi}$ is the root-mean-square Fermi-surface average of the gap and $\alpha$ is related to the *s*- to *d*-wave admixture with $\alpha=1$ pure isotropic piece and $\alpha=0$ pure angular-dependent piece. When for simplicity impurity scattering is introduced in Born approximation with the normal-state quasiparticle scattering rate given by $\pi t^+$, the renormalized gap and frequencies are given by[32]

$$\tilde{\omega}(\omega)=\omega+i\pi t^+\left\langle\frac{\tilde{\omega}(\omega)}{\sqrt{\tilde{\omega}^2(\omega)-\tilde{\Delta}_{sd}^2(\omega,\phi)}}\right\rangle_\phi, \tag{1a}$$

$$\tilde{\Delta}_s(\omega)=\Delta_s^0+i\pi t^+\left\langle\frac{\tilde{\Delta}_{sd}(\omega,\phi)}{\sqrt{\tilde{\omega}^2(\omega)-\tilde{\Delta}_{sd}^2(\omega,\phi)}}\right\rangle_\phi, \tag{1b}$$

$$\tilde{\Delta}_d(\omega)=\Delta_d^0 \tag{1c}$$

and the total renormalized gap is given by

$$\tilde{\Delta}_{sd}(\omega,\phi)=\tilde{\Delta}_s(\omega)+\tilde{\Delta}_d(\omega)\sqrt{2}\cos(2\phi). \tag{2}$$

Here $\langle\cdots\rangle_\phi$ denotes the Fermi-surface average. We note that the gap has now acquired a frequency dependence as is well known in the case of inelastic scattering.[33] The frequencies are also renormalized with $\tilde{\omega}(\omega)=\omega-\Sigma^{qp}(\omega)$, where $\Sigma^{qp}(\omega)$ is the quasiparticle self-energy to be distinguished from the optical self-energy[34–36] $\Sigma^{op}(\omega)$ that we will introduce later in our discussion. Equation (1) has been used in the past to describe the cuprates.[32] $YBa_2Cu_3O_{6+\delta}$ has chains as well as $CuO_2$ planes and this means that the in-plane superconducting gap can have a small *s*-wave component $\Delta_s^0$ in addition to a dominant *d*-wave part $\Delta_d^0$. As we will elaborate upon later, these same equations can be used in the context of the ferropnictides to describe a possible extended *s*-wave gap on the electron pocket located around the X point of the unfolded Brillouin zone (BZ). As described by Chubukov *et al.*,[13] in this case, an extended *s*-wave state referred to the X point rather than the center of the BZ will have the form used here, namely, $\Delta_s^0+\Delta_d^0\sqrt{2}\cos(2\phi)$, where $\phi$ is an angle defining momentum direction on the Fermi surface with origin taken at the X point. We consider only Born scattering which is simplest and has been used by Mishra *et al.*[26] in their discussion of the lifting of gap nodes by impurity scattering and its effect on the penetration depth. It is argued that when the two dopants are out of plane as is the case in some ferropnictides, weak scattering with significant small momentum-transfer components is expected. This is consistent with large intraband and weak interband scattering. As we are primarily interested here in the effect of the lifting of the nodes by residual scattering on the optical conductivity, we follow the lead of Mishra *et al.*[26] and neglect interband scattering. Such effects have been considered by Dolgov *et al.*[31] within the context of microwave and NMR relaxation rates. These authors also give results for more complicated impurity scattering such as the unitary limit. But these effects go beyond the scope of the present work.

There are many formulations of the complex optical conductivity,[32,37–39] $\sigma(T,\nu)$, at temperature $T$ which follows from the Kubo formula and can be written in the form[32]

$$\sigma(T,\nu)=\frac{\Omega_p^2}{4\pi}\frac{i}{\nu}\left\langle\int_0^\infty d\omega\tanh\left(\frac{\beta\omega}{2}\right)[J(\omega,\nu)-J(-\omega,\nu)]\right\rangle_\phi \tag{3}$$

with $\Omega_p$ the plasma frequency, $\beta=1/(k_BT)$, and

$$2J(\omega,\nu)=\frac{1-N(\omega,\phi)N(\omega+\nu,\phi)-P(\omega,\phi)P(\omega+\nu,\phi)}{E(\omega,\phi)+E(\omega+\nu,\phi)}+\frac{1+N^\star(\omega,\phi)N(\omega+\nu,\phi)+P^\star(\omega,\phi)P(\omega+\nu,\phi)}{E^\star(\omega,\phi)-E(\omega+\nu,\phi)},$$

where $\star$ indicates the complex conjugate. Here, $E(\omega,\phi)=\sqrt{\tilde{\omega}^2(\omega+0^+)-\tilde{\Delta}_{sd}^2(\omega+i0^+,\phi)}$, $N(\omega,\phi)=\tilde{\omega}(\omega+i0^+)/E(\omega,\phi)$, and $P(\omega,\phi)=\tilde{\Delta}_{sd}(\omega+i0^+,\phi)/E(\omega,\phi)$, and the average electronic density of states over the Fermi surface $N(\omega)/N(0)\equiv\langle N(\omega,\phi)\rangle_\phi$. In Eq. (3), vertex corrections are not included.

Before presenting results for the conductivity we note that in the pure case, $t^+=0$, the gap is given by $\Delta_0[\alpha+\sqrt{1-\alpha^2}\sqrt{2}\cos(2\phi)]$ in our extended *s*-wave model. A node exists in this function for $\alpha\leq\sqrt{2/3}$. In terms of the coefficient,

$$x=\frac{\alpha}{\alpha+\sqrt{1-\alpha^2}} \tag{4}$$

introduced in Ref. 32 as a measure of the amount of *s* wave relative to *s*+*d* wave, the critical value of $x$ for no nodes is $x_c=0.59$. For most of the graphs in the next section, $x$ was taken to be 0.5. Our extended *s*-wave model is the same as that of Mischra *et al.*[26] Their parameter $r\equiv\sqrt{2}\sqrt{1-\alpha^2}/\alpha=\sqrt{2}(1-x)/x$. In their work, they introduce a gap equation

with separable ansatz for the fixed anisotropy in the pairing potential. Solutions of this gap equation for various impurity concentrations give the corresponding change in critical temperature which is found to vary less rapidly with impurity-scattering rate than would be expected from magnetic impurities in an $s$-wave superconductor.[25] Here we take a somewhat different approach. We fix the gap amplitude $\Delta_0$ at a value of 12 meV and keep it fixed for all other calculations with $\alpha=1/\sqrt{2}$ or $x=0.5$. This means that at saturation impurities drop out of the gap equation because the gap defined as $\tilde{\Delta}(\omega)\omega/\tilde{\omega}(\omega)\equiv\bar{\Delta}_{sd}(\omega)$ has become isotropic, the gap $\Delta_s^0=8.5$ meV in our model. This gap corresponds to a critical temperature of 4.8 meV (55.7 K) since in an isotropic system the classic weak-coupling BCS gap to critical temperature ratio $2\Delta/(k_BT_c)=3.54$ applies. In strong coupling,[40] this ratio can be very different, of course. Assuming $t^+$ large enough that isotropy has been reached we have from Eqs. (1) and (2),

$$\bar{\Delta}_{sd}(\omega)=\frac{\Delta_s^0+i\dfrac{\pi t^+\bar{\Delta}_{sd}(\omega)}{\sqrt{\omega^2-\bar{\Delta}_{sd}^2(\omega)}}}{1+i\dfrac{\pi t^+}{\sqrt{\omega^2-\bar{\Delta}_{sd}^2(\omega)}}}.$$

Rearranging and canceling common factors gives

$$\bar{\Delta}_{sd}=\Delta_s^0=\alpha\Delta_0,$$

independent of frequency $\omega$ and a constant in momentum space (isotropic $s$ wave). Without impurities, the pure system critical temperature can be computed from the average gap $\Delta_0$ using the formula[41] $2\Delta_0/(k_BT_c)=3.54\exp(-\alpha_{2\ell})$ with $\alpha_{2\ell}=\langle\eta^2(\phi)\ln|\eta(\phi)|\rangle_\phi$, where $\eta(\phi)$ is the normalized gap anisotropy function $\eta(\phi)=\alpha+\sqrt{1-\alpha^2}\sqrt{2}\cos(2\phi)$ and $\alpha_{2\ell}$ works out to be equal to 0.3081 for $\alpha=1/\sqrt{2}$. This means that the average gap to $T_c$ ratio is 2.6 which is less than the isotropic BCS value of 3.54. Thus, anisotropy decreases this ratio but the maximum gap to $T_c$ ratio is actually greater than 3.54. For $\alpha=1/\sqrt{2}$ or $x=0.5$, we get

$$\frac{2\Delta_{\max}}{k_BT_c}=\frac{2\Delta_0}{k_BT_c}[\alpha+\sqrt{2(1-\alpha^2)}]=4.43.$$

For pure $d$ wave, these ratios are 3.027 and 4.28, respectively. In our case, the pure limit critical temperature is 107 K.

In Fig. 1, we present our results for the quasiparticle DOS in the superconducting state normalized to its normal-state value $N(0)$, i.e., $N(\omega)/N(0)$, vs $\omega$ for several values of the impurity-scattering parameter $t^+$. Here, $\pi t^+$ is the normal-state quasiparticle scattering rate $1/\tau^{qp}$ which is assumed to be constant. For these parameters, the pure limit gap has a maximum value of 20.4 meV and a minimum of −3.5 meV. Looking first at the solid (black) curve for which $t^+=0.2$ meV, we see two maxima corresponding to these extrema. The impurity content is small enough that there is little shift in these pure limit values. We note also the linear in $\omega$ dependence as $\omega\to0$ which reflects the node in the gap. For pure $d$ wave, the dependence would be $\omega/(\sqrt{2}\Delta_0)$ with

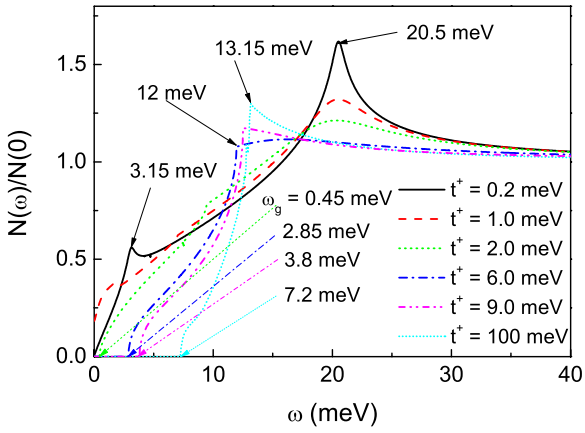


FIG. 1. (Color online) Normalized quasiparticle density of states $N(\omega)/N(0)$ in an extended $s$-wave gap superconductor with nodes vs energy $\omega$ for various residual quasiparticle scattering strength $\pi t^+$. Note that a gap develops at small $\omega$ when the impurity scattering is sufficiently large. Here $\Delta_0=12$ meV and $\alpha=1/\sqrt{2}$.

$\sqrt{2}\Delta_0$ the gap amplitude. For extended $s$ wave, we get instead $\omega/[\Delta_0\sqrt{2(1-3\alpha^2/2)}]$ which was derived under the assumption that there are nodes in the gap and that these dominate the value of the DOS as $\omega\to0$. This is only true for $\alpha<\sqrt{2/3}$. For $\alpha=0$, we recover the $d$-wave result. For $\alpha=1/\sqrt{2}$, as we have used here, we get $\sqrt{2}\omega/\Delta_0$, twice the well-known $d$-wave result. This formula agrees well with the numerical results of Fig. 1 for the (almost) pure case [solid (black) line]. This curve also agrees well with Fig. 4 of Mishra *et al.*[26] accounting for their slightly different choice of parameters $\Delta_0$ and $\alpha$. As we increase the impurity scattering, the two peaks noted above become smeared out and shift. Two features to be noticed are that as $t^+$ becomes very large, a spectral gap develops at low $\omega=\omega_g$. This is already seen in the dotted (green) curve for $t^+=2$ meV which corresponds to a impurity-scattering rate of about half the gap value. The upper energy peak which initially smears without moving its position in energy much starts to shift toward lower energies. First a shoulder develops and then this shoulder starts to become more peaked. Eventually, when $t^+\gg\Delta_0$, an inverse square-root singularity will develop at $\omega=\alpha\Delta_0$ (the isotropic limit) and $N(\omega)/N(0)=\mathrm{Re}[\omega/\sqrt{\omega^2-(\alpha\Delta_0)^2}]$, i.e., the DOS takes on its classic isotropic BCS value. This limit is not shown here and occurs only at unrealistically large values of the impurity-scattering rate much larger than the gap value $\Delta_0$. The last curve shown in Fig. 1 is for $t^+=100$ meV [short dotted (cyan) curve] and still displays some anisotropy. As discussed by Mishra *et al.*,[26] the low-$\omega$ evolution from linear in $\omega$ to a gap at $\omega_g$ changes the temperature dependence of the London penetration depth from linear in $T$ to thermally activated. The corresponding changes in $N(\omega)/N(0)$ are clearly large and should be measurable in tunneling. We would also expect corresponding large changes in the optical conductivity $\sigma(T,\omega)$ as a function of $\omega$ and this is the problem addressed in this paper.

## III. RESULTS

In Fig. 2, we show our results for the real part of the optical conductivity $\sigma_1(T,\omega)$. The temperature is $T=2$ K

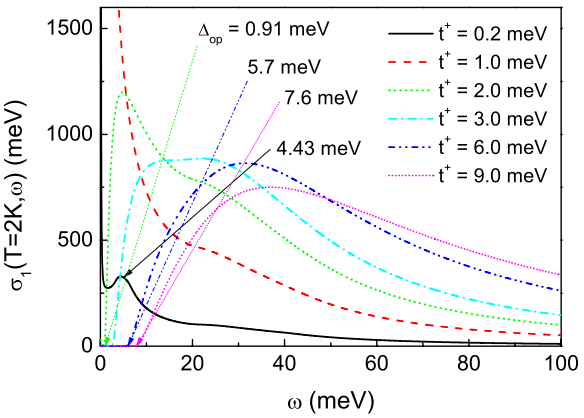


FIG. 2. (Color online) The real (absorptive) part of the optical conductivity $\sigma_1(T,\omega)$ vs energy $\omega$ and for various values of the quasiparticle impurity-scattering rate $\pi t^+$. The temperature is $T=2$ K. For cases when $t^+$ is sufficiently large to lift the gap nodes an optical gap $\Delta_{op}$ twice the value of the spectral gap energy $\omega_g$ of the previous section, develops at small omega and there is no absorption for $\omega \leq \Delta_{op}$. Here $\Delta_0=12$ meV and $\alpha=1/\sqrt{2}$.

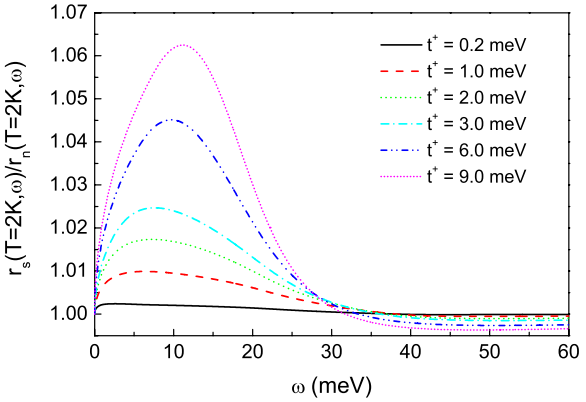


FIG. 3. (Color online) The ratio of superconducting state reflectance $r_s(T,\omega)$ vs $\omega$ at $T=2$ K to its normal-state equivalent $r_n(T,\omega)$ for various values of the impurity-scattering rate $\pi t^+$. Here $\Delta_0=12$ meV and $\alpha=1/\sqrt{2}$.

and various values for the impurity quasiparticle scattering rate $\pi t^+$ have been considered. We also set the plasma frequency $\Omega_p=1$ eV to be specific. The solid (black) line for $t^+=0.2$ meV is close to the pure limit. It has a small Drude peak about $\omega=0$ and shows evidence of the lower-energy peak seen in the corresponding DOS of Fig. 1 which was at 3.15 meV. In optics, the peak is at a higher energy (4.43 meV) as one would expect. While the DOS has another peak at 20.5 meV, no corresponding structure is seen in $\sigma_1(T,\omega)$ neither at twice this energy nor at the sum of the energies of lower and upper peak. As $t^+$ is increased, structures in $\sigma_1(T,\omega)$ evolve in a similar way to those noted in Fig. 1 for the DOS. In particular, a real quasiparticle gap at $\omega=\omega_g$ results in an optical gap $\Delta_{op}=2\omega_g$. Also, as we expect, $\sigma_1(T,\omega)$ rises out of this gap gradually. The short dotted (magenta) curve for $t^+=9$ meV is close to the well-known result for the dirty limit of Mattis and Bardeen.[30] We note also that the dashed-dotted (cyan) curve for $t^+=3$ meV shows a very flat maximum extending from almost 5 to 30 meV. This curve marks the transition from the peak-shoulder structure we see for $t^+=2$ meV to the "classical," almost $s$ wave, form we get for $t^+ \geq 6$ meV.

In optical experiments, it is the reflectance $r(T,\omega)$ which is measured directly and $\sigma(T,\omega)$ is a derived property. The relation between these two quantities is given by

$$r(T,\omega)=\left|\frac{1-\sqrt{\epsilon(T,\omega)}}{1+\sqrt{\epsilon(T,\omega)}}\right|^2, \quad \epsilon(T,\omega)=\epsilon_\infty+i\frac{4\pi\sigma(T,\omega)}{\omega}, \tag{5}$$

where $\epsilon(T,\omega)$ is the dielectric function and $\epsilon_\infty$ is its value at infinity. In what follows we set $\epsilon_\infty=1$ and, as before, $\Omega_p=1$ eV. Figure 3 gives the ratio of superconducting to normal-state reflectance $r_s(T,\omega)/r_n(T,\omega)$ at $T=2$ K for various values of elastic scattering. In the normal state, as is well known, the deviations below one of $r_n(T,\omega)$ increase with increasing $\omega$ as well as increasing values of $t^+$. On the other hand, at zero temperature, a BCS superconductor with isotropic $s$-wave gap cannot absorb for $\omega \leq 2\Delta_0$ and so becomes a perfect reflector. It is the competition between these two effects that determines how $r_s(T,\omega)/r_n(T,\omega)$ varies. The solid (black) curve for $t^+=0.2$ meV which corresponds to the clean limit is nearly one everywhere and shows little sign of superconductivity, except for a small rise above one at low $\omega$. This is the only observable feature associated with the onset of superconductivity, and, as is well known, the clean limit (little or no impurity scattering) is the wrong limit for observing such features. By comparison, the deviations in the short dotted (magenta) curve for $t^+=9$ meV are large. They are, however, somewhat different from what is found for ordinary isotropic $s$ wave which would show a rather steep drop as we go through $\omega=2\Delta_0$. Here, instead, the ratio shows a maximum at a frequency which is quite a bit larger than $\Delta_{op} \simeq 7.6$ meV but smaller than $2\Delta_0=24$ meV for this case (see Fig. 2) and only drops comparatively slowly above this energy before dipping below one at higher energies. It is clear that there are significant deviations in this particular quantity between isotropic BCS and the case of the lifting of the gap nodes in the extended anisotropic $s$ wave with nodes in the pure limit. These differences should allow one to differentiate between the two cases.

It has become standard in optical studies to extract from the optical conductivity an optical self-energy defined in terms of a generalized Drude form in which both, optical mass renormalization and optical scattering rate, acquire a frequency dependence. By definition of the complex optical self-energy $\Sigma^{op}(T,\omega)$, it is related to the conductivity $\sigma(T,\omega)$ by

$$\sigma(T,\sigma)=i\frac{\Omega_p^2}{4\pi}\frac{1}{\omega-2\Sigma^{op}(T,\omega)}. \tag{6}$$

It follows that

$$\omega-2\,\mathrm{Re}\,\Sigma^{op}(T,\omega)=-\frac{\Omega_p^2}{4\pi}\mathrm{Im}\,\sigma^{-1}(T,\omega) \tag{7}$$

and

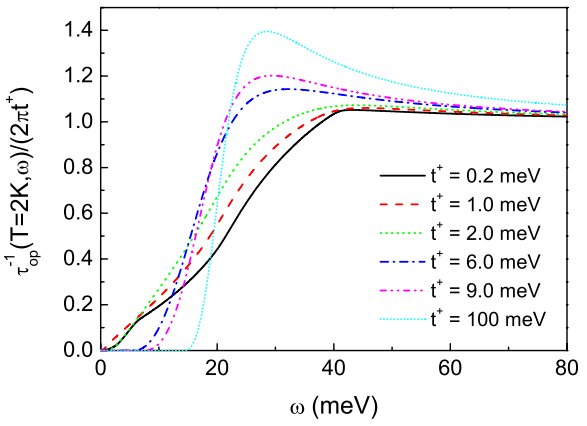


FIG. 4. (Color online) The optical scattering rate $\tau_{op}^{-1}(T,\omega)$ normalized to its normal-state value $2\pi t^+$ vs energy $\omega$ for $T=2$ K and various values of $t^+$. Here $\Delta_0=12$ meV and $\alpha=1/\sqrt{2}$.

$$-2\ \mathrm{Im}\ \Sigma^{op}(T,\omega)=\frac{\Omega_p^2}{4\pi}\mathrm{Re}\ \sigma^{-1}(T,\omega). \tag{8}$$

The optical mass renormalization $\lambda_{op}(T,\omega)$ is by definition $\omega\lambda_{op}(T,\omega)=-2\ \mathrm{Re}\ \Sigma^{op}(T,\omega)$ and the corresponding optical scattering rate $\tau_{op}^{-1}(T,\omega)=-2\ \mathrm{Im}\ \Sigma^{op}(T,\omega)$ which is the quantity most often discussed and which has been found useful in providing some physical insight into the meaning of the data obtained.

Results for the optical scattering rate normalized to its normal-state value of $2\pi t^+$ are given in Fig. 4 for $T=2$ K and various values of $t^+$. For the pure case where the quasiparticle DOS of Fig. 1 is linear in $\omega$ and finite for all $\omega\to 0$, we see absorption remaining to the lowest energy while in the case of large impurity scattering and a spectral gap (at $\omega_g$) in the DOS there is no absorption before $\omega=2\omega_g$. Impurity-scattering rates can clearly be used to determine details about the nature of the low-lying electronic excitations in an extended $s$-wave superconductor and their evolution with increased scattering rate. In particular, the lifting of the gap nodes has a clear signature.

## IV. MODEL FOR FERROPNICTIDES

Next we consider more specifically the ferropnictides. These are complex materials in which several bands cross the Fermi energy and there are holes as well as electron pockets. Among many others, the angular-resolved photoemission spectroscopy (ARPES) study by Zabolotnyy *et al.*[42] provides details on the topology of the Fermi surface in $Ba_{1-\delta}K_\delta Fe_2As_2$. Besides two concentric hole surfaces about the Γ point, one large and one small, they find a complex structure about the M point. The pocket centered at M is electronlike and is surrounded by four separate blades which are holelike forming a propeller-type shape. A minimum band-structure model for theoretical calculations and interpretation of experiment retains a single holelike band ($\alpha$) around Γ and an electronlike band ($\beta$) at M. In $Ba_{0.6}K_{0.4}Fe_2As_2$, Ding *et al.*[43] find from ARPES that the small Fermi surface at Γ has a superconducting gap of about

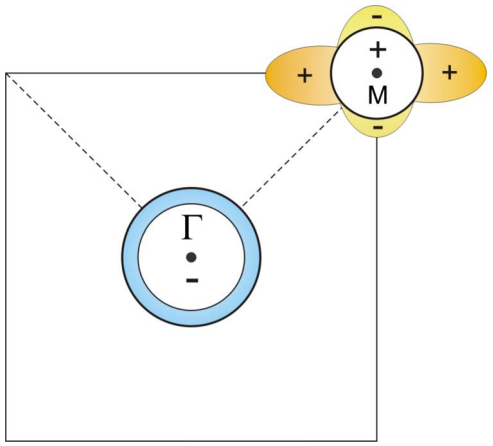


FIG. 5. (Color online) Sketch of the two Fermi-surface pockets in $k$ space, one about Γ (big Fermi surface) and one about M (small Fermi surface) represented by circles. The shaded rims are meant to represent an isotropic $s$-wave gap about Γ (blue) and an anisotropic extended $s$-wave gap about M (yellow).

12 meV while on the larger surface, it is 6 meV. The gap around M is close to 12 meV. Motivated by these findings the gap at Γ is assumed small and that at M big as we show schematically in Fig. 5. Here, for simplicity, we will assume as a model that the small gap is of isotropic $s$-wave symmetry while the large gap is extended $s$ wave. For the electron band centered at M, we take this point as the origin of momentum. In this coordinate system as shown by Chubukov *et al.*,[13] an extended $s$-wave gap then takes on the form of Eq. (1). This form is also used in the work of Mishra *et al.*[26]

The combined optical conductivity of the two bands is the sum of the two partial conductivities. If we denote the total plasma frequency by $\Omega_p$, we can introduce partial weights $w_1$ and $w_2$ with $w_1+w_2=1$ so that the separate band plasma frequencies are $\Omega_{p1}=w_1\Omega_p$ and $\Omega_{p2}=w_2\Omega_p$, respectively. In this notation, $\Omega_p$ is just an overall scale on the total conductivity and theoretical results for a single value of $\Omega_p$ need to be considered. Nevertheless, the total conductivity still depends on the choice of $w_1$ and $w_2$. This holds also for the optical scattering rate but not for the reflectance [Eq. (5)] which is not simply proportional to $\Omega_p$. In what follows we take $\epsilon_\infty=1$. Also for definiteness $\Omega_p=1$ eV and we take a residual scattering $t^+=2.5$ meV which corresponds to $\tau_{imp}^{-1}\simeq 16$ meV. These values are for illustration purposes only and are motivated by known experimental results. Yang *et al.*[44] quote a $\Omega_p\simeq 1.6$ eV and $\tau_{imp}^{-1}\sim 30$ meV. Tu[45] finds $\Omega_p=0.95$ meV and $\tau_{imp}^{-1}\sim 13$ meV. Finally, we set $\Delta_1=4$ meV and $\Delta_2=13$ meV and take $w_1=0.7$ and $w_2=0.3$ in one case [Fig. 6(a)] and the reversed in a second case [Fig. 6(b)].

Following these model assumptions, the weighted sum of the two individual bands complex optical conductivity $\sigma(T,\omega)=w_1\sigma^{(1)}(T,\omega)+w_2\sigma^{(2)}(T,\omega)$ gives the conductivity of the combined two-band system. Here $\sigma^{(1)}(T,\omega)$ and $\sigma^{(2)}(T,\omega)$ are the complex optical conductivities calculated using Eq. (3) for the two gap functions $\Delta_1(T,\omega)$ and $\Delta_2(T,\omega)$, respectively. In so doing we are assuming that there are no optical interband transition terms which is ex-

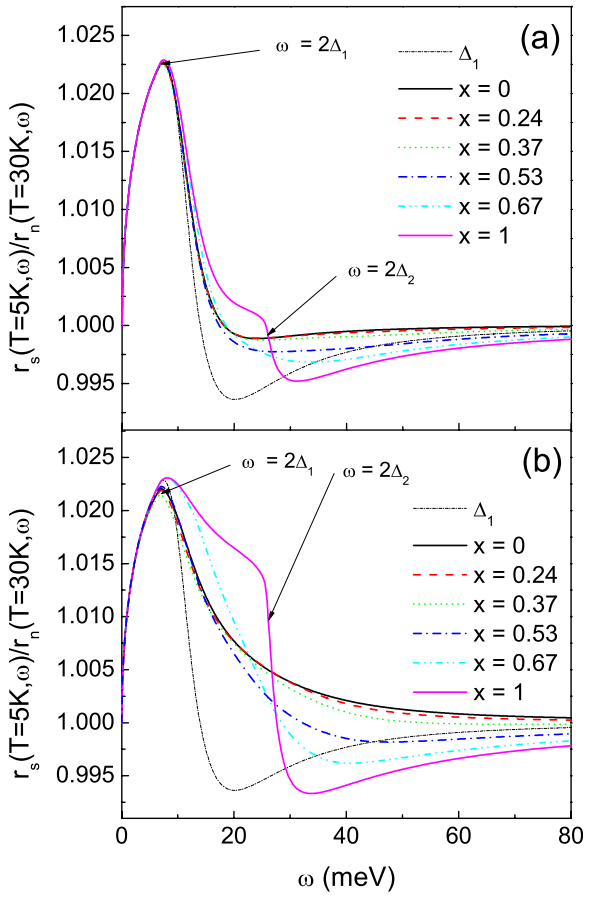


FIG. 6. (Color online) The reflectance ratio $r_s(T=5\ \mathrm{K},\omega)/r_n(T=30\ \mathrm{K},\omega)$ vs $\omega$ for different values of the anisotropy parameter $x$ in the big gap $\Delta_2$ at M. (a) The small gap at $\Gamma$, $\Delta_1=3.5$ meV (weight 70%), the big gap $\Delta_2=13$ meV (weight 30%), and the impurity-scattering rate $t^+=2.5$ meV. The light dashed-dotted (black) line gives the result for the isotropic $s$-wave gap $\Delta_1$ alone. (b) The same as above with the weights reversed.

pected since the two $\sigma^{(i)}(T,\omega)$ originate from very different regions of momentum space. The reflectance of the combined system follows from application of Eq. (5) to the combined $\sigma(T,\omega)$. It is clear that, in principle, there need not be a close relationship between the reflectance of the combined bands and the sum of the reflectance of each band separately. This will become clear below.

In Fig. 6(a), we present as a first result the reflectance ratio $r_s(T=5\ \mathrm{K},\omega)/r_n(T=30\ \mathrm{K},\omega)$ with $r_s(T=5\ \mathrm{K},\omega)$ in the superconducting state at $T=5$ K and $r_n(T=30\ \mathrm{K},\omega)$ the normal-state equivalent at $T=30$ K for the model described above. The $s$- to $d$-wave admixture in the large gap $\Delta_2$ is described by the parameter $x$, Eq. (4), with $x=0$ pure $d$-wave symmetry and $x=1$ pure isotropic $s$ wave. In the theoretical curves corresponding to this parameter between $0.67 \leq x \leq 1$, there are no nodes on the electron-pocket Fermi surface, i.e., there is a finite spectral gap in all momentum directions. Of particular interest is the (blue) dashed-dotted curve for $x=0.53$ because for this $s$- to $d$-wave admixture the gap $\Delta_2$ in a clean system would have nodes on the Fermi surface but for the assumed residual scattering $t^+=2.5$ meV these nodes are lifted by disorder and there is a small gap in the quasiparticle excitation spectrum. This $x$ value provides the transition between cases with a gap and without, i.e., with nodes. For orientation we added to the figure, the result for the isotropic $s$-wave gap $\Delta_1=3.5$ meV alone as the light short dashed-dotted (black) curve which has a peak at $2\Delta_1$ followed by a sharp drop and then a further dip below one, the hallmark of isotropic $s$ wave.

The introduction of a second larger gap $\Delta_2=13$ meV provides important modifications from the light short dashed-dotted (black) curve only for energies above the lower gap peak at $2\Delta_1=7$ meV. In particular, in all the other curves, the minimum around $\omega \simeq 20$ meV which dips below one is much shallower and shifted to higher energies. The short dotted (magenta) curve for $x=1$ which corresponds to an isotropic upper gap shows a shoulder followed by a second sharp drop at $\omega=2\Delta_2$. This drop allows one to identify by eye in the reflectance ratio a second energy-gap scale. No such prominent signature is present in the other curves. The results for $x=0$ [solid (black) line], $x=0.24$ [dashed (red) line], and $x=37$ [dotted (green) line] correspond to a second gap which is very anisotropic and has nodes on the M-point Fermi surface. These curves fall almost on top of each other and show only a very small and gradual rise toward their asymptotic value of 1 after the first maximum and sharp drop associated with $\Delta_1$ on the $\Gamma$ pocket. Thus, reflectance data cannot distinguish between such cases of extended $s$ wave with nodes and $d$ wave. As pointed out above, the next curve for $x=0.53$ [dashed-dotted (blue) curve] has a small spectral gap induced through impurity scattering which is sufficient to lift the nodes that would exist in the pure case. Although this curve dips below one more than do the results when nodes are present, the effect is not great. Nevertheless, there is a signature in all these cases of the presence of a second gap ($\Delta_2$). The relatively deep minimum at an energy just above $\omega=2\Delta_1$ characteristic of a small gap is entirely missing and this is true even for the dashed double-dotted (cyan) curve for $x=0.67$ which has a small gap everywhere on its Fermi surface at M. These results show that, unless both gaps are fairly isotropic, a detailed analysis of data is needed to determine the characteristics of the second gap $\Delta_2$. Also, the sign change in the $s^{\pm}$ model for superconducting gap symmetry cannot be determined from such measurements.

In Fig. 6(b), we show additional results for the reflectance ratio $r_s(T=5\ \mathrm{K},\omega)/r_n(T=30\ \mathrm{K},\omega)$ vs $\omega$ for the same gap and electronic-structure model that was used for Fig. 6(a) but we have reversed the weight of the gap admixture from 70% for $\Delta_1$ and 30% for $\Delta_2$ to 30% and 70%, respectively. As we see this has a significant effect on our results. Two distinct gap scales can still be seen in the short dotted (magenta) curve when both gaps are isotropic, i.e., $x=1$. In the opposite limit, when $\Delta_2$ has nodes, the runs for $x=0$, $x=0.24$, and $x=0.37$ remain close to each other and distinctly differ from the one gap ($\Delta_1$) BCS case [light short dashed-dotted (black) curve]. For the transition curve $x=0.53$ with nodes lifted by disorder [dashed-dotted (blue) curve] the variations are now larger than they were in Fig. 6(a) but no clear signature of the small spectral gap on the M pocket Fermi surface is easily identifiable.

In Fig. 7, we show the results for the real part of the optical conductivity $\sigma_1(T=5\ \mathrm{K},\omega)$ in millielectron volt vs $\omega$

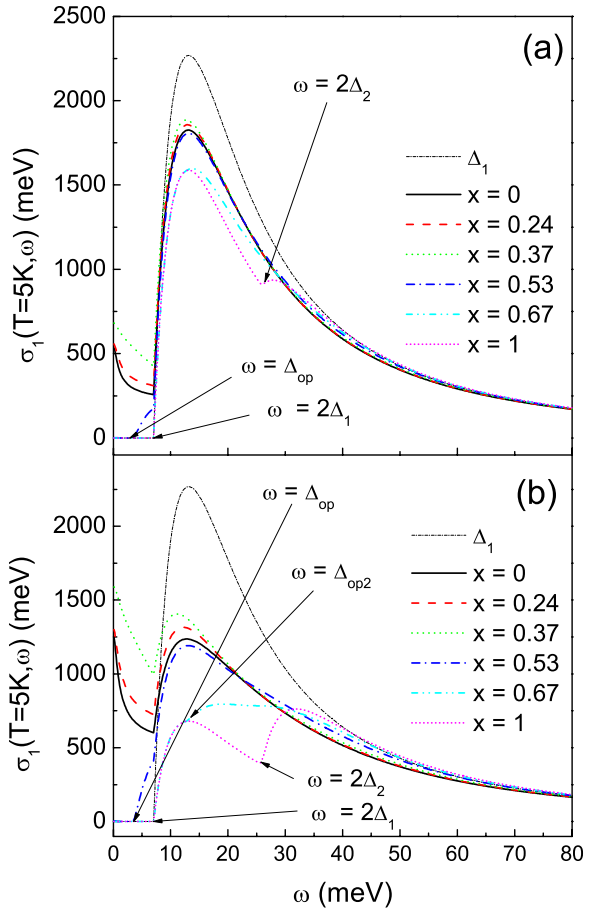


FIG. 7. (Color online) (a) The real part of the conductivity $\sigma_1(T=5\ \mathrm{K},\omega)$ in millielectron volt vs $\omega$ in millielectron volt for the same parameters as for Fig. 6 and for the weights 70% ($\Delta_1=3.5$ meV) and 30% ($\Delta_2=13$ meV). (b) The relative weights of the Γ and M pockets are reversed.

in millielectron volt for the same parameters as were considered in Fig. 6. Figure 7(a) is for $w_1=70\%$ and $w_2=30\%$ while Fig. 7(b) is for $w_1=30\%$ and $w_2=70\%$, the weights associated with the Γ and M pockets, respectively. Also shown for comparison [light short dashed-dotted (black) line] are the results for a single small gap $\Delta_1=3.5$ meV in which instance there is no absorption until $\omega=2\Delta_1$ at which point there is a sharp rise, followed by a peak and a slow drop toward the normal-state conductivity with which it merges for $\omega \gg 2\Delta_1$. When a second superconducting pocket around the M point is included there is now finite absorption below $\omega=2\Delta_1$. This absorption comes from the second large gap $\Delta_2=13$ meV for $x=0$ [solid (black) line], $x=0.24$ [dashed (red) line], and $x=0.37$ [dotted (green) line]. In these cases, $\sigma_1(T=5\ \mathrm{K},\omega)$ shows a small Drude-type peak centered around $\omega=0$. The boundary curve for $x=0.53$ [dashed-dotted (blue) line] shows, instead, zero absorption till $\omega=\Delta_{op}$ with $\Delta_{op}=3.4$ meV at which energy there is an absorption edge but this is small as compared with the main rise due to the first gap at $\omega=2\Delta_1$. For the case $x=0.67$ [dashed double-dotted (cyan) line] and $x=1$ [short dotted (magenta) line], the gap on the second pocket at M is sufficiently large that this second Fermi surface does not contribute to $\sigma_1(T=5\ \mathrm{K},\omega)$ until $\omega \geq 2\Delta_1$ (onset of absorption from the Γ pocket). Note the small kink at $\omega=2\Delta_2$ in the curve for $x=1$ which indicates the onset of added absorption due to the M pocket. Deviations in the absorption from a single gap at $\Delta_1$ are much more prominent in Fig. 7(b) which gives our results when $w_1=30\%$ and $w_2=70\%$, i.e., the gap $\Delta_2$ on the M pocket provides the dominant contribution to the real part of the conductivity. The Drude-type contributions to $\sigma_1(T=5\ \mathrm{K},\omega)$ for $x=0$, $x=0.24$, and $x=0.37$ are much larger than they were in Fig. 7(a). This is also true of the absorption onset in the dashed-dotted (blue) curve for $x=0.53$. For $x=0.67$, there is a small gap $\Delta_{op2}=13$ meV due to the M pocket which is seen as extra absorption at $\Delta_{op2}$. The contribution from each pocket individually is seen very prominently in the short dotted (magenta) curve for $x=1$ with isotropic gaps on both pockets. These considerations show that the real part of the optical conductivity derived from reflectance data is the better quantity to look at, when one is interested in the lifting of gap nodes by disorder in optical measurements.

In a recent paper, Muschler *et al.*[46] have provided experimental evidence for the lifting of nodes in the $Ba(Fe_{1-\delta}Co_\delta)_2As_2$ family using Raman scattering in moving from a sample with $\delta=0.061$ ($T_c=24$ K) to another with $\delta=0.085$ ($T_c=22$ K) they observed in the $B_{2g}$ response a change in low-energy behavior from linear in $\omega$ with zero, to a finite intercept with the frequency axis. While optics provides a different probe from Raman scattering it will be interesting to see if the analogous effect in optics as described in Fig. 7 confirms this interpretation of the Raman spectra.

## V. SUMMARY AND CONCLUSION

While theoretical studies indicate that the superconducting gap in the ferropnictides has extended *s*-wave symmetry, these states may be nearly degenerate in energy with *d*-wave states. Thus, small changes in doping or in some other parameter such as disorder produced, for example, by neutron irradiation or atom substitution, could lead to a change in gap symmetry within the same family of materials. Also an extended *s*-wave gap on one or more of the Fermi pockets could have nodes on its Fermi surface and these could be lifted by increased disorder. This was suggested by Mishra *et al.*[26] who were motivated in part by the confusing experimental observation that the low-temperature dependence of the London penetration depth of closely related samples can be different with some indicating a power law while others were more consistent with exponential activation.

In this paper, we have considered the case of an extended *s*-wave gap with or without nodes and also investigated how the lifting of the gap nodes through increased static impurity scattering presents itself in the optical properties. We found easily observable signatures of the opening of a finite spectral gap in the absorption (real) as well as in the reactive (imaginary) part of the optical conductivity. As the quasiparticle DOS evolves under increased disorder from linear in $\omega$, at small energies, to a gap (at $\omega_g$) and eventually acquires the characteristic coherence peak of *s*-wave superconductivity, the real part of the optical conductivity changes from a

*d*-wavelike response at $\omega \to 0$ with significant optical spectral weight remaining in this region to a gapped response which eventually tends toward that of a dirty *s*-wave Mattis and Bardeen form. Energies associated with extrema in the gap as a function of momentum produce peaks in the quasiparticle DOS. Structures corresponding to optical transitions which involve one of these peaks or between two such peaks can in some cases be identified in the optical conductivity. In addition, we find a signature of the lifting of gap nodes in the reflectance and in the optical scattering rate. In the specific case of the ferropnictides which we model here with two separate bands, one with a small isotropic gap, the second with a large extended *s*-wave gap, we find separate, easily identifiable signatures of each band in the reflectance ratio only when both gaps are isotropic. The signature of the small gap is a peak in $r_s(T,\omega)/r_n(T,\omega)$ at $2\Delta_1$ followed by a drop above this energy which, however, in contrast to single-band BCS does not drop below a value of 1, and can depend a lot on the percentage admixture between $\Gamma$ and M bands. This is followed by a second drop at $2\Delta_2$ and a dip below one. As anisotropy in $\Delta_2$ is turned on this second structure at $\Delta_2$ gets rapidly smeared out and its associated minimum becomes very shallow as the reflectance ratio tends toward 1. The reflectance of the combined bands is not the weighted sum of reflectances of the individual bands. On the other hand, the conductivities themselves are additive and the existence of a spectral gap in the extended *s*-wave order parameter of the electron band at M even when it is due to disorder, can be seen as a sharp absorption onset in its real part although for the case considered here this onset is not as prominent as it would be in the corresponding isotropic gap case. When there are nodes, some Drude absorption centered around $\omega = 0$ is expected instead.

## ACKNOWLEDGMENTS

This research was supported in part by the Natural Sciences and Engineering Research Council of Canada (NSERC) and by the Canadian Institute for Advanced Research (CIFAR).

*schachinger@itp.tu-graz.ac.at

[1] Y. Kamihara, T. Watanabe, M. Hirano, and H. Hosono, J. Am. Chem. Soc. **130**, 3296 (2008).
[2] D. J. Singh and M.-H. Du, Phys. Rev. Lett. **100**, 237003 (2008).
[3] E. J. Nicol and J. P. Carbotte, Phys. Rev. B **71**, 054501 (2005).
[4] H. J. Choi, D. Roundy, H. Sun, M. L. Cohen, and S. G. Louie, Nature (London) **418**, 758 (2002).
[5] A. A. Golubov, A. Brinkman, O. V. Dolgov, J. Kortus, and O. Jepsen, Phys. Rev. B **66**, 054524 (2002).
[6] L. Boeri, O. V. Dolgov, and A. A. Golubov, Phys. Rev. Lett. **101**, 026403 (2008).
[7] I. I. Mazin, D. J. Singh, M. D. Johannes, and M. H. Du, Phys. Rev. Lett. **101**, 057003 (2008).
[8] A. V. Chubukov, D. V. Efremov, and I. Eremin, Phys. Rev. B **78**, 134512 (2008).
[9] Y. Yanagi, Y. Yamakawa, and Y. Ōno, J. Phys. Soc. Jpn. **77**, 123701 (2008).
[10] K. Kuroki, S. Onari, R. Arita, H. Usui, Y. Tanaka, H. Kontani, and H. Aoki, Phys. Rev. Lett. **101**, 087004 (2008).
[11] F. Wang, H. Zhai, Y. Ran, A. Vishwanath, and D.-H. Lee, Phys. Rev. Lett. **102**, 047005 (2009).
[12] S. Graser, T. A. Maier, P. J. Hirschfeld, and D. J. Scalapino, New J. Phys. **11**, 025016 (2009).
[13] A. V. Chubukov, M. G. Vavilov, and A. B. Vorontsov, Phys. Rev. B **80**, 140515(R) (2009).
[14] P. G. Tomlinson and J. P. Carbotte, Phys. Rev. B **13**, 4738 (1976).
[15] H. K. Leung, J. P. Carbotte, D. W. Taylor, and C. R. Leavens, Can. J. Phys. **54**, 1585 (1976).
[16] H. K. Leung, J. P. Carbotte, and C. R. Leavens, J. Low Temp. Phys. **24**, 25 (1976).
[17] W. H. Butler, F. J. Pinski, and P. B. Allen, Phys. Rev. B **19**, 3708 (1979).
[18] C. O'Donovan and J. P. Carbotte, Physica C **252**, 87 (1995).
[19] C. O'Donovan and J. P. Carbotte, Phys. Rev. B **52**, 4568 (1995).
[20] C. O'Donovan and J. P. Carbotte, Phys. Rev. B **52**, 16208 (1995).
[21] D. Branch and J. P. Carbotte, Phys. Rev. B **52**, 603 (1995).
[22] G. Blumberg, A. Koitzsch, A. Gozar, B. S. Dennis, C. A. Kendziora, P. Fournier, and R. L. Greene, Phys. Rev. Lett. **88**, 107002 (2002).
[23] J. Mesot *et al.*, Phys. Rev. Lett. **83**, 840 (1999).
[24] S. V. Borisenko, A. A. Kordyuk, T. K. Kim, S. Legner, K. A. Nenkov, M. Knupfer, M. S. Golden, J. Fink, H. Berger, and R. Follath, Phys. Rev. B **66**, 140509(R) (2002).
[25] E. Schachinger, J. M. Daams, and J. P. Carbotte, Phys. Rev. B **22**, 3194 (1980).
[26] V. Mishra, G. Boyd, S. Graser, T. Maier, P. J. Hirschfeld, and D. J. Scalapino, Phys. Rev. B **79**, 094512 (2009).
[27] E. Schachinger and J. P. Carbotte, Phys. Rev. B **80**, 174526 (2009).
[28] K. Hashimoto *et al.*, Phys. Rev. Lett. **102**, 207001 (2009).
[29] C. Martin, R. T. Gordon, M. A. Tanatar, H. Kim, N. Ni, S. L. Bud'ko, P. C. Canfield, H. Luo, H. H. Wen, Z. Wang, A. B. Vorontsov, V. G. Kogan, and R. Prozorov, Phys. Rev. B **80**, 020501(R) (2009).
[30] D. C. Mattis and J. Bardeen, Phys. Rev. **111**, 412 (1958).
[31] O. V. Dolgov, A. A. Golubov, and D. Parker, New J. Phys. **11**, 075012 (2009).
[32] I. Schürrer, E. Schachinger, and J. P. Carbotte, Physica C **303**, 287 (1998).
[33] B. Mitrović, C. R. Leavens, and J. P. Carbotte, Phys. Rev. B **21**, 5048 (1980).
[34] E. Schachinger and J. P. Carbotte, Phys. Rev. B **62**, 9054 (2000).
[35] E. Schachinger, J. J. Tu, and J. P. Carbotte, Phys. Rev. B **67**, 214508 (2003).
[36] J. P. Carbotte, E. Schachinger, and J. Hwang, Phys. Rev. B **71**, 054506 (2005).
[37] E. J. Nicol, J. P. Carbotte, and T. Timusk, Phys. Rev. B **43**, 473 (1991).

[38] J. P. Carbotte, C. Jiang, D. N. Basov, and T. Timusk, Phys. Rev. B **51**, 11798 (1995).
[39] F. Marsiglio, J. P. Carbotte, A. Puchkov, and T. Timusk, Phys. Rev. B **53**, 9433 (1996).
[40] F. Marsiglio, R. Akis, and J. P. Carbotte, Phys. Rev. B **36**, 5245 (1987).
[41] H. Chi and J. P. Carbotte, Phys. Rev. B **49**, 6143 (1994).
[42] V. B. Zabolotnyy *et al.*, Nature (London) **457**, 569 (2009).
[43] H. Ding *et al.*, EPL **83**, 47001 (2008).
[44] J. Yang, D. Hüvonen, U. Nagel, T. Rõõm, N. Ni, P. C. Canfield, S. L. Bud'ko, J. P. Carbotte, and T. Timusk, Phys. Rev. Lett. **102**, 187003 (2009).
[45] J. J. Tu (private communication).
[46] B. Muschler, W. Prestel, R. Hackl, T. P. Devereaux, J. G. Analytis, J.-H. Chu, and I. R. Fisher, Phys. Rev. B **80**, 180510(R) (2009).